SPACE WEATHERING OF GENESIS MISSION SOLAR WIND COLLECTORS WITH INFERENCES FOR WEATHERING ON AIRLESS BODIES

Amy J. G. Jurewicz[1], Karen D. Rieck[2], Chad Olinger[3], Judy Allton[4], Mukul Sharma[5], Lindsay P. Keller[6], Roy Christoffersen[7]

1. ABSTRACT

Samples from the Genesis Solar Wind Sample Return (NASA Discovery 5) are a unique opportunity to study the initial stages of space weathering; i.e., the physical and chemical effects of solar wind irradiation. Arrays of collectors containing multiple materials were each exposed to a different solar-wind regime (fast, slow, bulk, or CME) at the L1 point for long durations (years). Materials exposed to the solar wind included metals, semiconductors, and insulators. Although the time of exposure was obviously short relative to samples having extra-terrestrial origins, optical properties, surface chemical properties, and matrix structure have changed in many collectors due to exposure to the solar wind. The thickness of amorphous zones, where present, appears to correspond with the depth of the peak of the solar wind H distribution in each regime. Damage from high energy particles was negligible because the collectors were 700 microns or less in thickness and shielded from the back by the spacecraft. Micrometeorite impacts and sputtering were also negligible because of the short exposure times. Our current results are preliminary: we hope future workers will extend this study both to support Genesis characterization efforts and to further understanding of space weathering processes on a geologic time scale.

[1] Corresponding author (Amy.Jurewicz@asu.edu) BCMS/SESE Arizona State University, Tempe AZ 85287-6004
[2] New Mexico Consortium, 4200 W. Jemez R., Suite 200, Los Alamos, NM 87544
[3] Department of Energy, AU-62, 19901 Germantown Rd, Germantown, MD 20875 USA
[4] Astromaterials Curation. NASA JSC, Mail Code XI2, Houston TX 77058
[5] Department of Earth Sciences, Dartmouth College, Hanover, NH 03755
[6] Mail Code XI, ARES, NASA Johnson Space Center, Houston, TX 77058
[7] Jacobs Engineering, Mail Code XI, ARES, NASA Johnson Space Center, Houston, TX 77058

2. SALIENT BACKGROUND ON THE GENESIS SOLAR WIND SAMPLE RETURN MISSION (NASA'S DISCOVERY 5)

The Genesis spacecraft flew to the L1 point and orbited for ~2 years, collecting solar wind for up to 853.82 days, then returning to Earth with its samples (Reisenfeld et al. 2013). The primary purpose of the mission was to enable measurement of solar wind composition in detail. The resultant data set is already being used for understanding topics in Cosmochemistry (e.g., the formation and history of planetary materials: see Meshik et al. 2007; McKeegan et al. 2011; Marty et al. 2011 as examples). But not all elemental and isotopic ratios in the solar wind exactly represent the solar Photosphere. Solar plasma is known to undergo fractionation during the formation of solar wind and acceleration away from the Sun. Thus, to ensure that all solar wind components measured in Genesis samples could be accurately and precisely corrected to true Photospheric compositional ratios, samples of four "regimes" of solar wind (slow, fast, coronal mass ejection, bulk) were collected during the flight. Elemental and isotopic ratios were expected to be unique to each sample as the solar wind of each regime was produced by a different combination of solar processes. The logic was that when (a)models of the processes involved in the solar wind formation and acceleration were correct for each regime, then (b) all regimes would give the same Photospheric composition. Thus, using Genesis data enables magnetohydrodynamic modeling of the processes that contribute to solar wind formation and acceleration (e.g., Laming et al 2017, 2019, Jurewicz et al. 2020) as well as independent checks of cosmochemical and/or astrophysical theories that are not founded on Genesis data (e.g., Bochsler 2007, Grimberg et al. 2006; Huss et al. 2020; Jurewicz et al. 2023). Therefore, the mission was expected to advance Solar Physics Research as well as Cosmochemistry.

What was neither expected nor wanted was for the Genesis collectors to contribute to the understanding of space weathering. The exposure time of the primary collectors to solar radiation was considered "short"; i.e., only ~2.3 years for the bulk SW collectors and less for the regime collectors (Reisenfeld et al. 2013). Cosmic rays (GCR and their SCR production) were measured on the spacecraft using a quartz block (Nishiizumi et al. 2006). But although high energy particles were present, they were not collected by the thin Genesis solar wind collectors. This can be shown using SRIM, a freeware program whose subroutine, TRIM, calculates implantation depth profiles

statistically using a Monte Carlo method (www.srim.org). SRIM indicates that a 30 MeV proton would pass though even the thickest Genesis "sapphire" (semiconductor-grade corundum) collector, as would a 10 MeV proton hitting the thickest Genesis silicon collectors. Thus, these high energy particles caused minimal damage to the Genesis solar wind collectors. Also, the temperatures each collector reached during solar exposure were relatively high because the expected exposure temperature was determined by the optical properties of the material (Jurewicz et al. 2003). For example, preflight "thermal vacuum" tests at the Jet Propulsion Laboratory (JPL) showed sapphire would equilibrate at about 55°C. Silicon (and probably diamond-like carbon films on silicon) would equilibrate at about 140°C to 160°C, with the temperature dependent on how the wafer was fabricated. Metal collectors would equilibrate at ~300°C. Finally, the diffusion of hydrogen, which comprises ~96% of the solar wind, was predicted to be high in the majority of the collector materials. *Therefore, it was assumed that many of the vacancies generated during implantation would diffuse or anneal during solar wind collection due to the combination of relatively high collector temperatures and low current of solar wind at the L1 point*. That is, pre-flight the science team believed that there would be minimal net damage to the collectors from the solar wind collection.

In fact, if all had gone as planned with the return of the Genesis samples, there would have been significantly fewer indicators for incipient "space weathering" caused by the solar wind exposure. Individual collectors would have returned intact, and the only observable contamination would have been the "brown stain", an organic film from spacecraft outgassing (first reported by McNamara and Stansbery 2005, detailed in Calaway et al. 2006), and aerosols deposited during relatively short duration exposures to air pre-launch and during atmospheric re-entry. These predicted contaminants would likely have been easily removed with a gentle cleaning or avoided through choice of analysis technique. But the Genesis Sample Return did not go as planned (McNamara 2005; Stansbery et al. 2005). Instead of floating through Earth's atmosphere on a parachute to be captured by helicopter, the Sample Canister, *sans* parachute deployment, augered into the desert floor and was breached. The Genesis collectors were both shattered and contaminated.

Since the crash, there has been an extensive amount of work focused upon learning to clean the surfaces of the various Genesis collector materials

without disturbing the subsurface solar wind layer (Allton et al. 2018). These careful cleaning and characterization studies showed that chemical and optical properties of the flown collector surfaces were different than the flight spare collectors. Moreover, solar wind components did not always behave as expected pre-flight. For example, silicon retained measurable SW H (Huss et al. 2012) and retained SW Fe (Burnett et al. 2007) both of which were predicted to diffuse based on the literature diffusivities compiled (by Allan Treiman) for the Genesis Feasibility Study. After 18 years of sample characterization and solar wind analyses, indicators have accumulated which point to physical, chemical, and optical changes in many of the collector materials due to solar wind exposure. Thus, studies of fragments allocated by Genesis Curation can provide important insights into the early phases of space weathering.

3. OBSERVATIONS

3.1. Separating Effects of the Crash from Effects from Exposure to Space

Before we present evidence for "space weathering", note that the effects of the crash were tremendous. Four-inch diameter hexagons were reduced to fragments. These small pieces were decorated with scratches, cracks, deposited splotches of aluminum, smeared bits of other collectors, steam created from damp (saline) soil at the crash site – the list is endless. Macroscopic changes can be seen by in the pictures of samples of the catalog on the Genesis Curation website (https://curator.jsc.nasa.gov/genesis/). But, by deduction, most effects of the crash could be separated from chemical and physical changes acquired during the flight. For example, the germanium solar wind collector (Ge) analyzed contained reduced amounts of solar wind, especially the amount of shallowly implanted He (Heber et al. 2008; Heber et al. 2009). Heber et al. attributed the lower amounts of solar wind in Ge to diffusion at collection temperatures. However, there is physical evidence that Ge containing solar wind may have been lost during the uncontrolled re-entry and crash. The small size of the recovered Ge fragments, their often slightly rounded edges, and the ubiquitous Ge aerosol on the surfaces of the spacecraft suggest etching. That is, an O- plasma may have formed during heating as the Sample-return Capsule plummeted to Earth and, in germanium collectors, this plasma etched the collection surface along with a portion of

the solar wind. In contrast, the "brown stain" was inferred to be the product of spacecraft outgassing during flight (e.g., Calaway et al. 2006). It tended to be found on cooler areas of the spacecraft and in regions adjacent hardware in which lubricants or adhesives were present. For example, it was thick on the edge of the bulk solar-wind collector that capped the array deployment mechanism (ADM) which was stabilized in its location using a silicone-based adhesive (Grimberg et al. 2008). Finally, optical properties of many flown collectors are different from those of their flight spare counterparts (Calaway et al. 2009, Allton et al. 2022). Although contaminant films can cause optical changes, they were clearly not the cause of all post-flight changes in optical properties (Calaway et al. 2009). Thus, it was inferred that the collection process itself could change optical properties of solar wind collectors; i.e., there was some space weathering.

"On airless bodies, the term 'space weathering' has been generally been *[sic]* adopted to represent a suite of processes that serve to slowly alter regolith properties" (from Grier & Rivkin 2018). This "space weathering" usually includes many drivers such as solar wind, high-energy solar and cosmic rays, micrometeorite impacts. On Earth, drivers for weathering include wind, water, and temperature changes, etc. When Genesis samples show changes in optical properties due to exposure to space, the processes that effected these changes were limited to those driven by solar wind.

Thus far, the space-weathering processes inferred to have affected Genesis collectors can be binned into three categories: (1) redistribution of the solar wind after implant (i.e., deviation from the SRIM-calculated distribution - a diffusive process); (2) surface chemistry changes(a mix of chemical and physical processes); and (3) changes in optical properties resulting from space exposure (coupled physical, chemical, and diffusive processes).

3.2 Redistribution of the Solar Wind after Implant

Of course, diffusion is a process that can happen for any element in any material given the right conditions and enough time. Here, we look at enhanced diffusivity driven by radiation damage. Enhanced diffusivity of ions during implantation has been observed for more than half a century (e.g., Dienes & Damsk 1958). The classic scenario is "radiation enhanced diffusion".

Radiation enhanced diffusion is when point defects generated by the implanting ion move to a free surface and then disappear. Since the defects have charge, implanted ions may move with them. Typically, this process causes either a loss of material from the implant or exchange of implanted material with contaminants on a free surface. When the excess defects are destroyed, radiation-enhanced diffusion ends.

The second scenario is "radiation-enhanced segregation". In radiation-enhanced segregation an implanted area of the lattice has enough damage that it becomes a low energy sink for impurities. Diffusion moves some elements towards that damaged area (usually the implanted ion), while other elements – usually matrix ions -- may diffuse away. The net effect is a change in local composition without a gain or loss of material in the system. In hindsight, radiation-enhanced segregation appears to overwhelmingly dominate depth profiles measured in Genesis silicon samples. However, both processes have been proposed for Genesis silicon samples and the evidence will be reviewed below.

3.2.1. SW Mg from Two Genesis Collectors

Magnesium was one of the first elements measured in Genesis samples. SW Mg is relatively abundant, and Mg is stable in silicon (Portsel et al. 2020). But, the SW Mg depth profile in silicon did not have the shape predicted by SRIM. Thus, "radiation enhanced diffusion" in Genesis silicon was proposed by B. King (University of Newcastle, Australia) at the March 2006 Genesis Science Team meeting. In King et al. (2008), that initial idea was detailed, and their calculations indicated exchange of SW Mg with the collection surface. Later, measurable exchange of SW Mg was disproved *(Burnett unpublished; Jurewicz et al. 2021, Heber et al. 2021)*, when the amount of SW Mg was measured in both silicon and diamond-like carbon (DLC) on silicon (DoS) collectors and found to be identical within error. Note that Mg in diamond-like carbon does not show any radiation-enhanced diffusion or segregation, so SW Mg depth profiles have the shape predicted by SRIM (e.g., the supplement of Jurewicz et al. 2020 gives example profiles with fits).

Since SW Mg was conserved in silicon despite radiation-enhanced movement, what King (and others) had observed was radiation-enhanced segregation. SW Fe

measurements were also equivalent in silicon and DoS collectors. SW Fe depth profiles were skewed profiles in silicon but calculable using SRIM in DoS.

3.2.2. Segregation in Laboratory Implants

Shapes of multi-ion laboratory implants into silicon were compared by Koeman-Shields et al. (2017). Part of their implant was ^{1}H + $^{24,26}Mg$ (with all species effectively having the same peak) and part of the implant was left anhydrous. Mg depth profiles were then measured using secondary ion mass spectrometry (SIMS). The depth profiles were different shapes in the hydrous and anhydrous regions of the same sample. Specifically, the Mg depth profile in the anhydrous region looked almost gaussian, as expected. The Mg depth profile in the H implanted region was narrower, with more Mg on the surface-side of the implant peak – somewhat consistent with the expected shape of the H-implant.

Koeman-Shields et al. (2017) considered the difference in the hydrous and anhydrous depth profiles to have been either an artifact of the order of implantation or uneven sputtering in the H-bearing region during SIMS analysis. On the other hand, it could also be a sign of implanted Mg moving towards H-bearing silicon to achieve a metastable equilibrium. Therefore, these results are consistent with radiation-enhanced segregation.

3.2.3. SW H in Genesis Silicon

The relevance of Koeman-Shields et al. (2017) to flown silicon collectors is complicated. Laboratory implants use ion currents orders of magnitude higher than solar wind, and the silicon substrate is much cooler than exposed Genesis silicon collectors. The solar wind was collected for years at collection temperatures of 140° – 160° C (Reisenfeld et al. 2017; Jurewicz et al. 2003). The shape of the SW H depth profile in returned Genesis silicon has not been measured as SW depth profile measurements have been done to forward Genesis objectives, not to explore space weathering. Literature diffusion coefficients (e.g., Jones 2000) had suggested that the first-implanted H ions would move centimeters. Moreover, the measurement is difficult and expensive. First, SW H is usually in the transient region during front-side depth profiling, so the collector would need to be thinned for back-side depth profiling. Second, the low H concentrations mean time-consuming preparations of the instrument (e.g., bake-out and pumping). Thus,

a lot of preparation is needed to measure the shape of a solar wind implant for an element whose fluence is not expected to represent the total amount of implanted solar wind collected.

One experiment measured the SW H profile in Genesis silicon indirectly. First, an ideal SW H depth profile in silicon was modeled in SRIM using the SW H energy spectrum derived from Advanced Composition Explorer spacecraft data. Sharma et al. (2022) then combined this SRIM model with the measured SW H fluence (Huss et al. 2020) to calculate expected Solar Wind Proton concentrations as a function of depth (**Figure 1** x-axis). Finally, they plotted their experimentally determined etching rates for two Genesis-flown

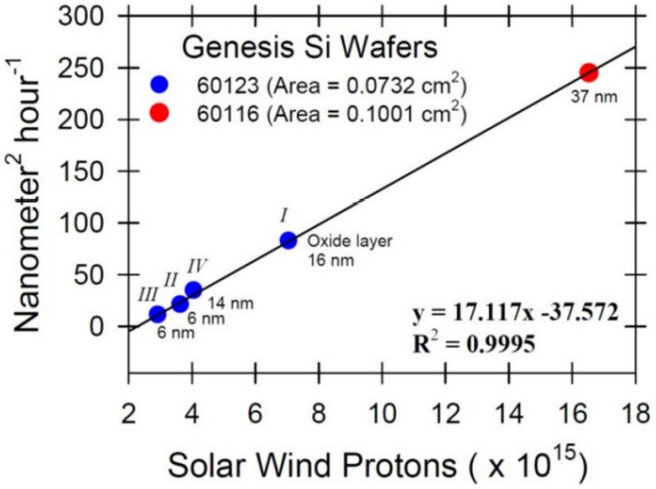

Figure 1. Results from Sharma et al. (2022) showing that their stepwise etching for cleaning Genesis Bulk SW silicon collectors appears to be controlled by SW H. X-axis is the SW H concentration profile predicted using SRIM. Their etching technique requires the repeated, controlled formation of Si oxide using nitric acid followed by an HF etch.

samples (markers in **Figure 1**) as a function of the SW H. Etching rates were determined measuring the ratios of Nd isotopes implanted into the samples. Surprisingly, this model indicates how SW H implanted into silicon can be used to explain near-surface etching rates in silicon collectors. The straight line in **Figure 1** is the correlation of etch rate with calculated SW H concentration, $R^2 = 0.9995$. The chemical formula for the etching was given in the abstract as:

$$Si + zh^+ + (4-z)H^+ \rightarrow Si^{4+} + \left(\frac{(4-z)}{2}\right) H_2 \qquad (1)$$

where z is the number of electrons removed during oxidation of Si that combine with H^+ to produce H_2 gas and h^+ represents the holes created by electrons. Note that the Sharma et al. (2022) model is based on SRIM, it assumes no diffusion of SW H in the Genesis silicon. So, Sharma et al. (2022) suggests that some (if not most) of the SW H remained as implanted despite the high temperatures and long duration of the collection period. However, it

does not address whether the implanted SW H controls the diffusion of the other implanted species.

Figure 2 addresses whether SW H may have controlled movement of SW ^{24}Mg in the Genesis silicon samples, similar to the effect in Koeman-Shields et al. (2017). In **Figure 2a**, SW ^{24}Mg data (orange markers with power-law extrapolation to surface) of Heber et al. (2014) is compared with a SW ^{24}Mg SRIM calculation (purple line) and the SW H SRIM calculation (red dashed line). As in the experiment of Koeman-Shields et al. (2017) from Calaway et al. 2009: i.e., that vacancies generated by the SW implant control the radiation-enhanced movement in Genesis samples (e.g., King et al. 2008; Calaway et al. 2009). The trends are model defect intensities from different solar wind sources (details in caption). Note that the shape of the SRIM SW H implant in **Figure 2a** fits more of the measured SW ^{24}Mg profile than any of the shapes generated by models of SW defect concentrations in **Figure 2b**.

3.2.4. Redistribution of SW in Genesis Silicon

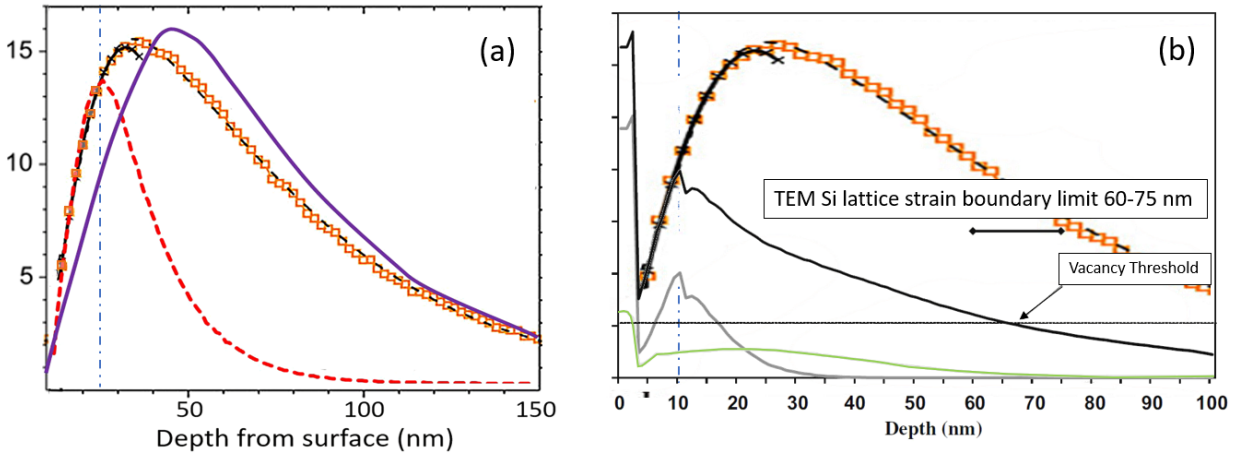

Figure 2. *Comparison of the measured near-surface shape of the SW ^{24}Mg implant with SRIM models for* ***(a)*** *SW H and* ***(b)*** *SW vacancies. Note: the SRIM models have the same depth scale as the SIMS data but were scaled vertically to give best fits to the SW ^{24}Mg SIMS data. Symbols: both* ***(a)*** *and* ***(b)****: orange squares and black power-law fit is from Heber et al. (2014) Figure 10. Vertical blue dashed line is the maximum extent that the models shown fit the shape of the SIMS data 25 nm vs. 10 nm for* ***(a)****,* ***(b)****, respectively.* ***(a)****: purple line is the SRIM calculated SW ^{24}Mg implant; red dashed line is the SRIM calculated SW H implant.* ***(b)****: Black, dark grey, and light green profiles are SRIM-calculated defect calculations for SW implants (H, He, C, O Ne, Mg, Si, Fe), SW H, and SW He, respectively from Calaway et al. (2009) Figure 12. These calculations using models analogous to King et al. (2008), but with more detail for the solar wind implant. Specifically, the Calaway et al. (2009) model uses the known radiation environment as determined from instruments on both Genesis and Advanced Composition Explorer (Reisenfeld et al. 2007).*

The previous sections in 3.2 showed that, although the solar wind exposure caused some radiation-enhanced movement, elements were retained. In fact, H -- which was supposed to diffuse rapidly -- could be modeled using SRIM. The SRIM program does not allow for diffusion after implantation, so accuracy of the SRIM model indicates little movement of at least a subset of implanted SW H ions. However, the processes of radiation-enhanced diffusion and radiation-enhanced segregation are not mutually exclusive. For example, SW Na fluences measured in silicon were significantly different from those measured in DoS collectors (Rieck 2015). In addition, back-side SIMS depth profiles of SW ^{23}Na and SW ^{24}Mg measured concurrently in bulk solar-wind collectors always seemed to end at different points in silicon depth profiles; however, when measured concurrently in DoS, the SW ^{23}Na and SW ^{24}Mg had the same "surface breakthrough" point (Rieck et al. 2021). This "early breakthrough" seen for SW Na (both in Rieck 2015 and Heber et al. 2014 and 2021) is consistent with diffusion controlled by the defect model presented in **Figure 2b**.

Although likely rare, situations like that observed for SW Na indicate that every analysis of an element or isotope should be verified in a second Genesis collector type if possible (Burnett et al. 2019).

In silicon, why might Na exchange with the free surface whereas Mg or Fe might not? There is little reason for any element to move from the low-energy segregation layer, if there is a lattice site/defect that can accommodate it (e.g., Portsel et al. 2020 on Mg diffusion). Therefore, any element implanted into Si that makes a silicide under reducing conditions (e.g., Mg, Fe) is likely to be extremely stable in that relatively disordered portion of the lattice. Similarly, any element that requires a significant activation energy to move through crystalline silicon would be unlikely to diffuse *en masse* away from the low-energy layer and through the crystal to a free surface. On the other hand, Na is an easily mobilized element whose silicide is less stable and might not be fully accommodated in that disordered region.

3.3 Surface Chemistry Changes

After the crash, it was necessary to clean the surfaces of flown wafers without disturbing the solar wind. Development of cleaning procedures often began with implants into flight spare materials to check for deleterious

effects of implant damage, but researchers invariably shifted to using flown samples for their tests. Not only were the types of contamination from the crash beyond what was readily duplicated in the laboratory, but the implanted flight spare material did not respond to surface cleaning treatments like flown samples.

The most striking change in surface chemistry due to space exposure is shown in studies by Janakiraman Paramasivan et al. (2018) and Sharma et al. (2022). Using Nd isotopes as a tracer in implanted silicon SW collectors, they used the implanted SW H to control the surface-etching performed in a series of oxidation/dissolution steps. This study was discussed above in Section 3.2 (see text and **Figure 1**).

Another distinct chemical difference between flown and unflown Genesis material was observed by Humayun et al. (2011) in the SW collectors known as SoS (for silicon on sapphire). SoS is a ~190 nm thick layer of silicon epitaxially grown on R-plane-oriented sapphire (corundum) substrates. While working on a very aggressive acid cleaning technique, Humayun et al. (2011) report:

> *"We explored the use of a hot conc. HF treatment on Si and SoS control wafers: these control wafers emerged shiny from hot HF after an overnight emersion, with negligible weight loss of the Si. This process was later used on implanted SOS controls, with the same result. To remove residual silicate hosts of Mg on flight wafers, we performed the same HF treatment; however, the flight SoS wafers reacted rapidly with complete removal of the silicon layer after 2 hours, terminating further cleaning of these wafers."*

No detailed "postmortem" examination was conducted to understand the striking difference in the surface chemistry of flown versus flight spare SoS. But, since the SoS surfaces etched used HF, the Si films were likely oxidized. Remember that the silicon wafers studied by Sharma et al. (2022) were protected from oxidation by retention of SW H (**Figure 1**). If so, and if this oxidation happened during the crash, then a SW H as modeled by Sharma et al.

(2022) was not present in any of the SoS fragments. Perhaps flexing and microcracking of the SoS allowed O to bypass the hydrogenated Si layer? If so, why didn't oxidation occur in silicon during the crash: Heber et al. (2021) reported reasonable SW O abundances from silicon collectors.

On the other hand, it is possible the oxidation was a sign that different processes affected silicon and SoS collectors during flight. Perhaps the polished surface of silicon wafers had amorphous areas that retained SW H while, in the unpolished Si layer of SoS, the SW H diffused during SW exposure as expected pre-flight. Or, there may have been more of a driving force for diffusion of SW H in SoS because Si was only present as a thin layer. A layer of silicon might allow SW H to easily diffuse to the Si/Al_2O_3 interface (which, by definition, is composed of defects) rather than diffusing into an "infinite" low-defect crystal.

Understanding why flown SoS surfaces differ from those of flight-spare fragments of both silicon and SoS requires future study, preferably by transmission electron microscopy (TEM).

3.4 Changes in Optical Properties resulting from Space Exposure

Optical ellipsometry using a Woollam M-2000 spectroscopic ellipsometer was designated by Genesis Curation, pre-flight, as a technique needed for characterizing flown collectors. This method was selected for its demonstrated ability to observe and characterize any thin films that might have deposited on the collectors from spacecraft outgassing. Data from ellipsometry does not directly measure the structure or composition of a thin film or surface layer. Rather, the technique measures shifts in polarization (amplitude and phase) of a known beam of light as it reflects off the sample. These observed polarization shifts are then modeled by assuming material parameters for the reflective surface being studied. Roughness, composition, film thickness, etc., are often gleaned from these models, but answers can be non-unique. Therefore, the resultant materials characterization is only as accurate as the information assumed in the model (see tutorial at www.jawoollam.com for a detailed overview).

Ellipsometry characterization of the flight samples began soon after they arrived at the Johnson Space Center (JSC). Models indicated that there were changes in some Genesis collectors that were not well modeled by assuming

that the collectors represented flight spare samples coated with an organic film (Calaway et al. 2009). Accordingly, it was inferred that radiation-damage during solar-wind collection had changed the optical characteristics of at least some types of flown samples: i.e., the near-surface structure of the flown samples was not the same as the structure of the flight-spare samples. To produce accurate models from the ellipsometry data, the near-surface structure of flown samples needed to be characterized. So, Genesis Curation requested that the Transmission Electron Microscopy Laboratory at JSC perform reconaissance investigations to characterize any physical structures in flown collectors formed during solar wind collection.

Calaway et al. (2009) published the first compilation of TEM observations made at JSC. They studied a Genesis bulk silicon collector and presented detailed TEM photomicrographs, energy-dispersive spectra (EDS) and compositional maps, as well as defect models (e.g., **Figure 2b**) for what they had observed. This was the only prior Genesis study from JSC to discuss "space weathering" of Genesis samples in a refereed journal. Since then, Genesis Curation, in collaboration with their colleagues in the JSC TEM laboratory, has done more work, including: (a) further TEM on Genesis bulk solar wind silicon collectors, (b) a TEM section of a slow-speed solar wind silicon collector, and (c) a TEM section of a bulk solar wind Genesis sapphire collector. The results of these studies were published as Lunar and Planetary Science abstracts. The main observations they report are as follows.

3.4.1 Bulk SW Silicon Collector

An example TEM photomicrograph from Calaway et al. (2009) is given in **Figure 3**. Note that welded to the collection surface of the collector being studied is a small grain of silicon "dust"; i.e., powdered silicon derived from collectors pulverized during the crash. When a particle of Si dust impacts an intact silicon collector it can "weld" to reduce its surface energy. From this TEM micrograph, it is not possible to tell if the amorphous silicon (a-Si) in this bit of silicon "dust" was (1) a feature of a pulverized collector or if (2) the a-Si formed from energy input into the surface of the Si dust grain by the crash itself. The underlying silicon substrate does not have an amorphous layer. However, it is possible that the near-surface damage in the substrate is extensive enough that it is near the threshold of a-Si

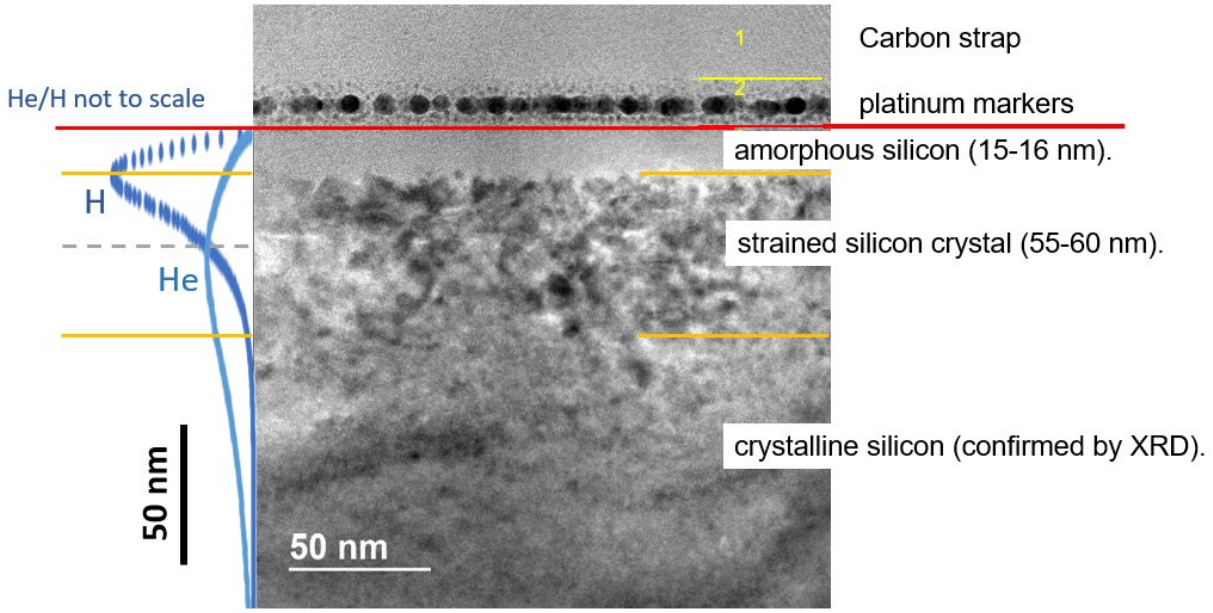

Figure 4. A TEM section through a bulk solar wind silicon collector from Allton et al. (2019). An a-Si layer is located just below the SiO_2 surface (red line). The thickness of the a-Si is the same as the depth from the surface to the theoretical peak of the SW H implant. Note: the ratio of He/H in the plot (LHS) is exaggerated for the reader. The ratio of the areas under the SW He and SW H curves should be 0.0391 (Reisenfeld et al. 2013).

formation. Note: a-Si forms when, after sufficient radiation damage, it nucleates on the native oxide layer of the silicon wafer and grows inward (Titov et al. 2003).

Figure 4 is also a TEM section into a bulk silicon collector. The collector fragment is free of visible crash debris and obvious physical damage from the crash. It also, quite definitely, has an amorphous silicon layer, which lies between the intrinsic SiO_2 layer (covered by red line) and strained silicon (formed by solar wind collection). Not enough TEM work on flight-spare silicon has been performed to know if an amorphous layer due to polishing existed on some portions of the collectors prior to flight. What is clear is that the SRIM-calculated peak position of the SW H implant in the bulk sample is at the same depth as the bottom of the a-Si layer. So, in this TEM section, the peak of the SW H appears to be the threshold damage where the a-Si layer stops thickening.

3.4.2. Slow SW Silicon Collector

A TEM cross-section through the SW zone of a silicon slow-speed solar wind collector is in **Figure 5** (after Allums et al. 2020). Just like the bulk SW collector, this sample has an amorphous zone extending from the oxide layer to the calculated peak of the SW H implant. The SW H peak depth correlates with the bottom of the a-Si layer even though the peak of the slow solar wind H (14.0 nm) is slightly different from that of the bulk SW H (15.6 nm). Note: solar wind peaks were calculated using the SRIM code developed by C. Olinger in 2017 (Olinger et al. 2018). Then the peak of the model was calculated by fitting the curve with a 6-order polynomial and calculating where the derivative, dx, equaled 0. Exposure time for the slow solar wind collector was also shorter: 333.67 days, or about 39% of the exposure time of the bulk solar wind collectors (Reisenfeld et al. 2013).

Again, only one TEM section of a slow solar wind collector was presented, and no check for an amorphous polishing zone was made on preflight wafers. But there is one definite difference between this TEM section of a slow solar wind collector (**Figure 5**) and the two bulk solar wind collectors in **Figures 3** and **4**. Specifically, **Figure 5** does not show as much significant lattice damage (strained silicon) extending from the amorphous layer to ~65-75 nm seen in the two bulk SW collectors. Clearly more samples need to be observed in the TEM before any conclusions are drawn. However, Reisenfeld et al. (2013) points out that, in the slow portion of the solar wind, SW H and SW He velocities are closer than for bulk solar wind (in which He tends to be faster; e.g., their Fig. 5). The He/H ratio is also smaller. These facts may explain the difference in texture between slow and bulk solar wind collectors.

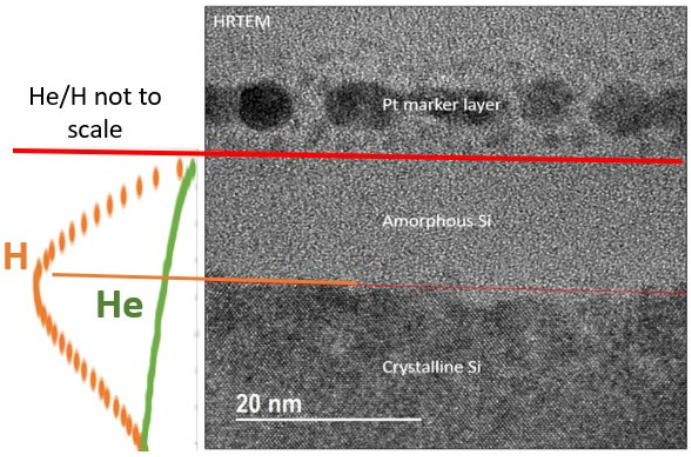

Figure 5. TEM cross section of slow solar wind silicon collector with the position of the low-speed SW H and SW He marked. The SW He / SW H intensities (LHS) are exaggerated: the He/H ratio measured by the ACE spacecraft was 0.0369 (Reisenfeld et al. 2013). In this TEM section, the amorphous layer is thinner than the one for the bulk collector in **Figure 4**.

3.4.3. Bulk SW Sapphire Collector

The semi-conductor grade "sapphire" used as a Genesis solar wind collector was laboratory grown single-crystal corundum cut so that the polished face has an R-plane (1102) orientation. The only TEM section from a flown Genesis sapphire collector thus far is a bulk solar wind collector (**Figure 6**). Like the bulk solar wind silicon in **Figure 4**, there is a damaged surface layer (somewhat analogous to the amorphous layer in the weaker silicon structure

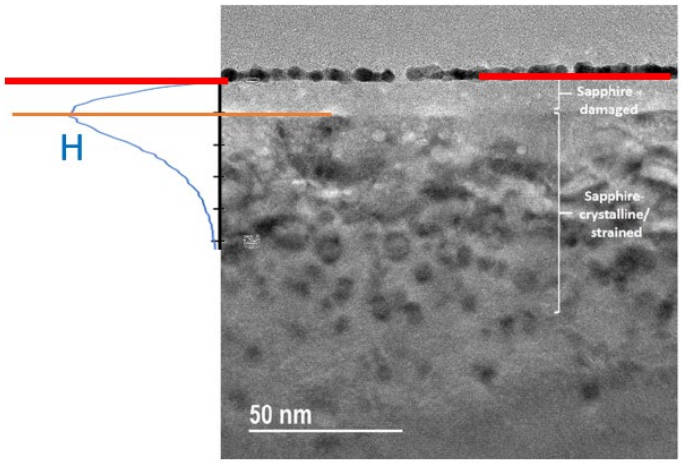

Figure 6. TEM of bulk solar wind sapphire collector presented in Keller et al. (2022) with the solar wind H depth profile shown using the same depth scale on the LHS. This collector is from the same regime as the Si collectors in **Figures 3** and **4**, but the SW H implant shown here was modeled using the structure and density of sapphire.

but partially nanocrystalline) that extends from the surface to the peak of the SW H implant (10.2 nm). Below that layer is strained (disrupted) crystal extending another ~75 nm into the crystal. Sapphire can be "amorphized" by ion beam implantation in the laboratory under some circumstances with, perhaps, both defect structures and implanted ions playing a role (e.g., Flynn et al. 2012, Abe et al. 1997). However, there has been little work on pre-flight and unexposed Genesis sapphire, so it is unclear how much (if any) of the damaged (nearly amorphous, nanocrystalline) and strained layers in the flown sapphire are due to polishing. It is unlikely that stresses from polishing would create such equant defects in the lattice. The overall geometry of the damage is consistent with that observed in bulk solar wind exposed silicon (**Figure 4**) in that: a) the nanocrystalline layer extends to the SW H peak and then stops, and b) the underlying damage is about 50 - 80 nm deep. If this texture was caused -- even in part -- by radiation damage, it is a definite step towards explaining the difference in optical properties between flight-spare and flown samples observed using ellipsometry.

4. DISCUSSION

518
519 4.1. Radiation Damage in Genesis Collectors
520
521 It is clear from the observations above that some combination of chemical and
522 structural changes occurred in the silicon and sapphire exposed to the solar
523 wind. Ellipsometry also showed that these changes significantly skewed the
524 optical properties of many flown collectors. At least in silicon, diffusion
525 of the implanted solar wind H did not occur to the extent predicted pre-
526 flight, since there appears to be H-control of surface processes which mimic
527 the H-implant geometry modeled by SRIM (**Figures 1 and 2a**).
528
529 The most striking physical feature noted post-flight, present in most of the
530 TEM sections, was the amorphous layer in the silicon and the equivalent
531 nanocrystalline layer in the sapphire. It is not yet known if these layers
532 were present pre-flight as only a few flight-spare collectors have been
533 sectioned for TEM. However, when present post-flight, these layers of
534 amorphous material always seemed to stretch from the surface to the
535 calculated peak of the solar wind H implant, regardless of the solar wind
536 collection regime. Further TEM studies of both flight-spare and Genesis-flown
537 materials are required to validate that the observed correlation is robust.
538
539 The amorphous layer surprised researchers, because the Genesis Mission design
540 had implicitly assumed that collectors would not be exposed to enough solar
541 wind necessary for the amorphization of silicon or space-weathered natural
542 minerals (e.g., Calaway et al. 2009). But, if amorphization was not initiated
543 by the solar wind during flight, then perhaps an amorphized layer formed
544 during the polishing of the wafer surface. If so, when present it appears to
545 have acted as a nucleation site for further growth of a-Si (or quasi-
546 amorphous sapphire). That is, a pre-existing amorphous layer could
547 hypothetically have acted as a sink for the accumulating near-surface damage
548 to the substrate caused by the implantation of SW H. It is also possible that
549 the implanted SW H diffused more slowly in pre-existing amorphous (or
550 nanocrystalline) layers than in areas of damaged crystal that did not have an
551 amorphous layer. If so, then a pre-existing amorphous layer from polishing
552 might have retained enough SW H to cause hydrolytic weakening of the crystal
553 structures of both silicon and sapphire, lowering the activation energy
554 needed for growth of that amorphous/nanocrystalline layer. Retention of H in

555 a pre-existing amorphous layer may be responsible for the observations
556 presented in **Figure 2**.
557
558 Retention of SW H in an amorphous silicon layer would be consistent with the
559 observation that radiation-enhanced segregation was not observed in the
560 amorphous, anhydrous diamond-like carbon collectors (see supporting online
561 material of Jurewicz et al. 2020). Radiation damage to a crystal
562 fundamentally changes crystal structure but, under the same conditions, an
563 amorphous material can just stay amorphous. It also suggests that the
564 retention of solar wind can change the intrinsic chemistry of a crystalline
565 surface because amorphous near-surface material is a separate phase with its
566 own chemical properties.
567
568 So, the eventual position of implanted solar wind ions is typically more
569 complicated than modeling by SRIM (e.g., **Figure 2**) or using diffusivities
570 reported in the literature. There may be radiation-enhanced segregation
571 (e.g., **Figure 2a**) or a phase change (amorphization) may, unexpectedly, create
572 new, metastable positions for implanted ions. For example, SW H and SW Fe did
573 not diffuse as expected at the ~140° - 160°C collection temperature.
574 Extrapolating Jones (2000) diffusivities to 150° C (using their Table 1.4 and
575 Figure 1.23) indicates SW H and SW Fe should have diffusivities of 4E-7 cm^2/s
576 and 5e-10 cm^2/s, respectively. Then, assuming $x=\sqrt{(4Dt)}$, the initially
577 implanted SW H and Fe should have moved about 108 mm and 3.8 mm,
578 respectively, during collection! This prediction is in stark contrast to the
579 results presented in **Figures 1 and 2** for SW H, and equivalent abundance of SW
580 Fe in silicon and DoS collectors (e.g., Burnett et al. 2007).
581
582 It can be argued that the lack of diffusion was due to a pre-existing
583 amorphous layer. But, if not, were the first H ions implanted immobilized?
584 That is, did they bond strongly with silicon by satisfying defects in the Si-
585 bonds in the crystal lattice caused by the implantation? As an example: Mg
586 diffuses rapidly in silicon when it does diffuse. But it also forms bonds in
587 silicon that make it difficult for Mg to remain ionized, so any diffusion
588 tends to be transient (Portsel et al. 2020). Or, perhaps, H ions were
589 stabilized by anchoring defect clusters and these relatively large clusters
590 were reasonably stable in the silicon lattice? In any case, **Figure 1**
591 suggests the formation of a local static equilibrium -- some recombination of
592 ions and damage from the implantation that created a local energy well, so

593 that there was minimal diffusion of SW H ions in the Genesis silicon under
594 collection conditions.
595
596 Thus, this view of the radiation-enhance segregation as a local, metastable
597 equilibrium explains why Jurewicz et al. (2021) found the same ^{24}Mg fluences
598 in both Si and DLC within measurement error while the defect models of
599 Calaway et al. (2009) and King et al. (2008) predicted that the bulk solar
600 wind ^{24}Mg would exchange with the collection surface. Even though there are
601 occasions when Mg diffuses relatively rapidly in silicon (Jones 2000)
602 diffusion tends to be quenched by the interaction of the Mg impurity with the
603 crystal lattice and corresponding defects. That is why exchange of solar wind
604 with the collection surface (or surface impurities) was not observed by
605 Jurewicz et al. (2021). In contrast, SW Na mostly stayed in the silicon
606 lattice but appears to have had some exchange with the surface (Rieck et al.
607 2021). Na is easy to ionize and tends to stay ionized in silicon. Perhaps
608 this is because sodium silicide is relatively unstable, has a monoclinic
609 crystal structure and significantly different stable bonding directions than
610 c-Si. SW Na is also present at a much lower concentration than Mg in the
611 solar wind, so a net exchange of a small number of Na atoms would be more
612 noticeable. Thus, any artifact of ion movement following the predictions of
613 Calaway et al. (2009) and King et al. (2008) should be considerably easier to
614 recognize in SW Na fluences rather than, say, SW ^{24}Mg fluences.
615
616 As an important aside for Genesis researchers: since the heavier SW Mg
617 isotopes (^{25}Mg and ^{26}Mg) are implanted slightly deeper than SW ^{24}Mg (i.e.,
618 kinetic energy = ½ mv^2 where the velocity, v, of each isotope is the same, but
619 increased mass, m, gives increased energy and momentum = mv), surface
620 exchange *may* affect the measurement of SW Mg isotopes in silicon at the
621 permil level. So, isotopes must be checked in a second collector material.
622
623 Finally, how do we explain the rapid dissolution of flown silicon-on-sapphire
624 collectors when etched in concentrated HF (Humayun et al. 2011)? Hydrofluoric
625 acid is used regularly in the semiconductor industry to remove oxide films
626 and, often, to leave a layer of Si-H on the surface that tends to passivate
627 further oxide growth. It is also used on amorphous silicon for the same
628 reason. The flight-spare SoS and the silicon wafers did not dissolve under
629 the same conditions.
630

One potential difference between the silicon of SoS versus a silicon wafer is that SoS collectors were not subjected to a polishing step pre-flight. Thus, the SoS definitely did not have a pre-existing amorphous layer. If the amorphous silicon is what allowed the polished silicon wafers to retain H under the Genesis exposure conditions, then all SW H should have diffused from the SoS as predicted. If so, the SoS surface would have been radiation damaged, but would not have SW H present to protect it from oxidation upon re-entry. There are likely other differences between silicon wafers and the silicon of SoS, too, such as crystal orientation, and the presence of a boundary layer (the sapphire interface) in SoS that could accommodate diffusion of SW H. Thus, answering in detail why the silicon of the SoS etched so quickly in concentrated HF will require TEM work and, perhaps, lab experiments.

4.2 Relevance of this Study to Space Weathering in General

Although preliminary, the study of Genesis samples thus far may give insight into understanding space weathering on asteroidal (and other) materials exposed to solar wind in the solar system. **Figure 7** compares the physical features of Genesis samples with space weathering on Itokawa (after Thompson et al. 2014). The three TEM sections are: a Genesis bulk solar wind sapphire **(Figure 7a)**, a Genesis slow solar wind silicon **(Figure 7c)**, and a space-weathered orthoclase grain from the asteroid Itokawa **(Figure 7b)**. Although from three different publications, these microphotographs have been stretched and cropped to the same scale so that features can be compared directly.

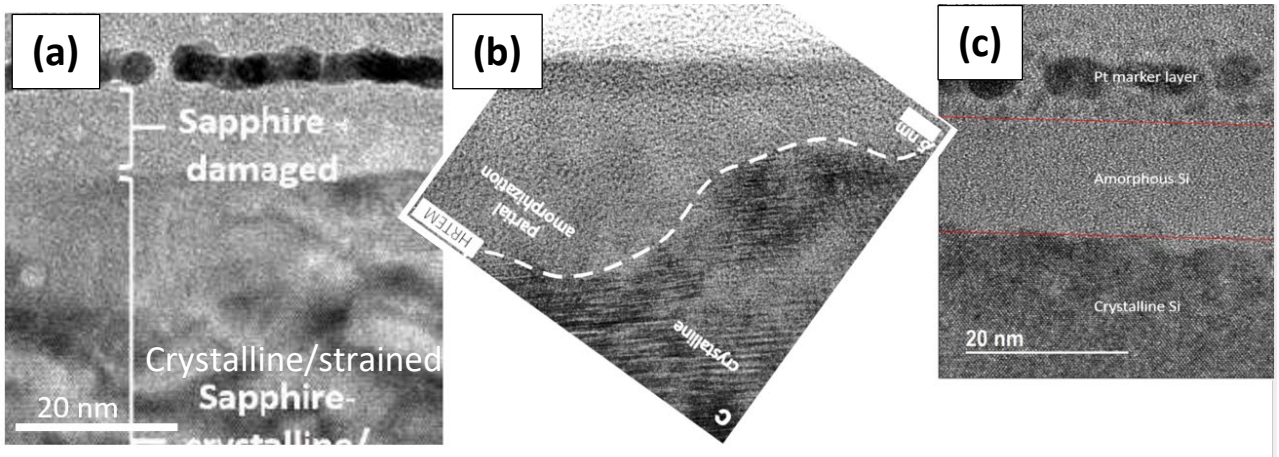

Figure 7. TEM photomicrographs of (**a**) Genesis sapphire (after Keller et al. 2022), (**b**) returned orthoclase from asteroid Itokawa (after Thompson et al. 2014), and (**c**) Genesis slow solar wind Si (after Allums et al. 2020). Note: **(a)**, **(b)** and **(c)** are scaled to the same magnification.

All three of the TEM micrographs have near-surface layers that are either damaged (nanocrystalline), partially amorphous-, or amorphous. In both **(a)** and **(c)** it is not yet known if these near-surface layers predated the solar wind irradiation or if they were formed in place. However, the thickness of these layers corresponds to the depth of the peak of the SW H implant. The TEM section in the Itokawa orthoclase grain **(b)** has a partially amorphous layer. It is not uniform, but nonuniformity would be expected if it were partially shadowed during exposure or, perhaps, the grain occasionally rolled during its time on the surface of Itokawa. It is also plausible that an unrelated active weathering process, such as a micrometeorite impact or even falling debris, added energy locally, which allowed the amorphous layer to thicken in that region.

From **(a)** and **(c)** it can be inferred that the partially amorphous layer on the Itokawa sample probably nucleated on the surface when there were sufficient near-surface defects due to accumulated damage from solar wind H (Titov et al. 2003 for details on an experimental formation of an amorphous layer in silicon; Abe et al. 1997 and Flynn et al. 2012 discuss formation of amorphous alumina on sapphire during ion irradiation). That layer then, initially, thickened to the depth representing the peak of the SW H implant as did the Genesis samples. Unlike the Genesis samples, the grain from Itokawa may have been exposed to solar wind for millennia; if so, sputtering probably removed some of the original surface. (Note that sputtering of the collection surface is negligible in Genesis samples because of the short exposure times). That said, solar wind is likely to have accumulated significantly faster than sputtering during the long-term exposure of the Itokawa grain. The amount of solar wind ions implanted (as well as damage accumulated) probably increased over the entire implant profile with time. Thus, the concentration of defects and ions which initially defined the peak of the SW H in the lattice will be found at deeper levels with time. This increase in deep solar wind damage will allow thickening of the partially-amorphous layer (see Fig. 3 of Titov et al. 2003 for the analogous process in silicon).

Comparing other features of Genesis samples with space-weathered natural samples can also produce insights into the process of space weathering. For example, the bulk solar sapphire in **Figure 7(a)** and the bulk solar wind silicon in **Figure 4** both have a zone of visible damage and strain below their respective nanocrystalline and amorphous layers. In contrast, both the

Itokawa grain and the slow SW Genesis silicon have a mostly crystalline, relatively undamaged region below their respective partially-amorphous and amorphous layers. If bulk solar wind collectors have a damaged region below their amorphous zone, why should the Itokawa grain not have a strained/damaged zone below the partially-amorphous layer -- like the Genesis slow solar wind collector (**Figure 7c**)?

Genesis slow and bulk solar wind collectors captured the low-speed solar wind concurrently. However, slow solar wind collectors were stowed when the solar plasma had higher velocity components, but bulk solar wind collectors were still deployed. Thus, Genesis slow solar wind collectors sampled a much more uniform velocity solar wind than bulk collectors and there was less dispersion between the SW H and SW He velocities than for bulk SW (Reisenfeld et al. 2013). Similarly, the Genesis solar wind collection experiment was at Earth's L1 point while the Itokawa grain collected "bulk" solar wind further from the Sun (i.e., the asteroid belt). Thus, the "bulk solar wind" that irradiated Itokawa was comprised of a tighter spectrum of SW H + SW He velocities than bulk solar wind at the L1 point of the Earth-Sun system (Reisenfeld et al. 2001) because the velocity of SW He slows down with distance from the sun so that its velocity becomes closer to that of SW H near the asteroid belt. The fact that the Itokawa grain has more features in common with Genesis slow solar wind than bulk solar wind may reflect the extent of the variation of the velocities of ions within the solar wind flux.

4.3 Space Weathering as a Progression of Metastable Equilibrium Conditions

Section 3.2 outlined why the current information we have on Genesis samples is consistent with the idea that the formation of space weathering may be described as a series of metastable equilibrium conditions. This progression is diagramed in **Figure 8**. If there was a pre-existing amorphous layer caused by polishing on some of the Genesis wafers (e.g., **Figures 4, 5 and 6**), then the texture that we observed in those samples was jump-started to Step 3 in **Figure 8**. Similarly, those without the amorphous layer (like the substrate in **Figure 3**) would be somewhere in the continuum of Step 2 in **Figure 8**. If the amorphous/semi-amorphous layers had been formed in flight by radiation damage, then **Figure 3** would represent a material very close to the threshold of Step 3.

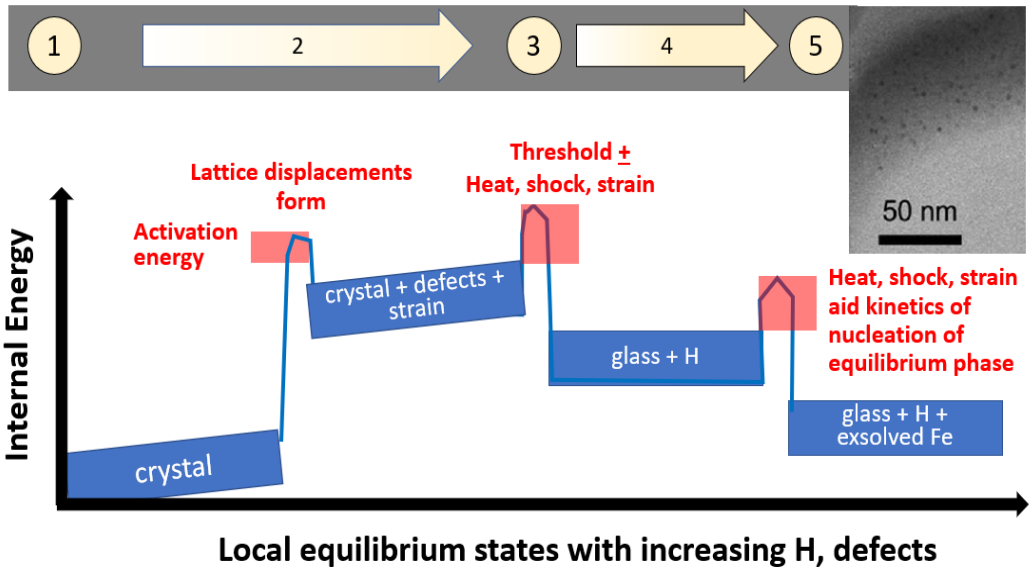

Figure 8. Cartoon illustrating a hypothetical process for the formation of space weathered surfaces. Here, space weathering is formed by continuously increasing the concentration of SW H and defects. Markers in the grey banner refer to corresponding numbered steps in the text. Blue blocks in the diagram give the expected morphology of the weathering surface. Red blocks represent "thresholds" between metastable equilibrium states (i.e., states when there is sufficient activation energy is accumulated to drive a change of morphology). They are left as "humps" as kinetics may delay rearrangement of atoms to a lower energy state. Red suggests sources/sinks of energy other than solar wind (e.g., impact, high energy ions) that may increase kinetics to enable nucleation of the new "phase" or feature quickly at low temperatures. Microphotograph inset at upper right is modified from Grier and Rivkin (2018).

Each stage in **Figure 8** represents a crystalline matrix adapting to the energy imparted by different concentrations of defects and implanted ions. In each stage, the matrix should have different physical (and likely optical) characteristics reflecting its metastable, static equilibrium state. Optical characteristics are most strongly affected when the space weathered material is rich in iron especially when the space weathered rim has precipitated iron spherules (e.g., inset in upper right of **Figure 8** from Grier and Rivkin (2018). Although there is no iron-rich Genesis collector material, the process illustrated in **Figure 8** would likely lead to precipitation of Fe metal as increasing H lowers the intrinsic oxygen fugacity of the crystal. The Fe-metal produced would form spheres due to surface energy effects, and the size of the spheres would depend on diffusion rate and the number of nuclei present. Note that an outside source of energy, such as a micrometeorite impact, would do more than raise the local temperature.

Diffusion rates would increase, and if no significant O was emitted by the impact, Fe-metal would stabilize at lower H concentrations (i.e., higher oxygen fugacity see Hirschmann 2021). Heating would be sudden, so spherules would form more quickly, probably at fewer nucleation sites, and spherules would likely be larger than those without additional energy added by impact. Observations and experiments concerning nanophase and microphase iron globules are discussed in Grier and Rivkin (2018).

Details of the hypothesis as diagrammed in **Figure 8** are as follows:

1. Prior to solar wind exposure on an airless body, the crystal is in a low energy state. Although there may have been some internal damage (e.g., acquired by cosmic ray exposure) perhaps even before accretion.

2. This step deals with damage to the crystal as its energy state increases. It can be thought of as being divided into two parts. First, point defects are formed. After a damage threshold is reached, point defects coalescence to form strained lattice, dislocations, and related features visible using TEM.

   The initial exposure to solar wind deposits energy into the crystal lattice, damaging it with vacancies and interstitials. The excess energy deposited by the solar wind is calculable *if* assumptions are made about concurrent diffusion and atomic rearrangements. Most of the energy deposited by solar wind resides just below the crystal's surface (see Figure 11 of Calaway et al. 2009). Much of the damage is concentrated near the crystal's surface as well (see **Figure 2b**).

   With some low-energy implantation, the chemical potential for diffusion is strongest towards the surface because: (i) there are more damage pathways near the surface due to implantation; (ii) the surface itself is more accommodating to impurities physically and chemically. And, at least in silicon, amorphization requires a threshold dose of damage at the surface (Titov et al. 2003). But the chemistry between contaminants and the crystal, stress gradients at the surfaces of crystals, photon-induced charges at the surface, etc., must also be taken into consideration to determine the distribution and mobility of both impurities and defects.

In contrast, high-speed solar wind components might slow the formation of an amorphous layer or strain in the crystal because they would create point defects at significant subsurface depths. Although, in general, the chemical potential gradient pulling defects and ions into the depths of the crystal is weaker than the near-surface gradient, it will have more influence on diffusion at depth in the crystal. So, if implanted far enough from the surface, both ions and excess defects from the irradiation may diffuse towards the baseline energy state of the unirradiated, deep crystal lattice.

Towards the middle of Step 2, there is a point where diffusion alone cannot dissipate enough of the changes to the crystal lattice. At this threshold, the crystal tries to lower its internal energy with modifications to the crystal structure that would be visible in a TEM section. A locally, lower energy state is achieved by gradually forming clusters of defects around interstitials. Still, the lattice is strained, which can cause dislocations that eventually coalesce to further reduce the energy of the damaged crystal (e.g., **Figure 3**).

3. Eventually, the radiation damage near the surface increases to the point where portions of the crystal lattice are no longer stable with respect to an amorphous, or partially amorphous, material. Step 3 is the threshold where this new material can nucleate. On silicon the point of nucleation appears to be the native oxide layer (Titov et al. 2003), but the partially amorphous nature of the layers in the Genesis sapphire and the Itokawa orthoclase grain (**Figure 7**) suggests that a combination of the free surface (e.g., Flynn et al. 2012) and agglomerated dislocations in the near-surface portion of the crystal lattice may be nucleation points in other crystal types. This threshold can be achieved by irradiation only, but micrometeorite impacts, collisions, heating, etc., may expedite the process.

4. The new amorphous (or partially amorphous) surface layer can accommodate the incoming solar wind ions and their related damage with little post-implantation diffusion (e.g., **Figure 2** and discussions in Section 3.2 of this text). Solar wind accumulates in this amorphous region over time, increasing the local H/O ratio since solar wind is

~96% H. Eventually the intrinsic oxygen fugacity (partial pressure of O relative to other gases, mostly H) will decreases until it is below where Fe-O and Fe-Si bonding is destabilized, and Fe precipitates (at moderate temperatures this "threshold" partial pressure of O in a gas phase defines the "iron wüstite buffer"). Fe precipitation is likely to occur at scattered nucleation points (inset upper RHS of **Figure 8**) and will lower the local internal energy. However, the sudden addition of energy (e.g., heating or shockwaves from a nearby micrometeorite impact, or perhaps concentrated high-speed SW from an intense solar flare) could facilitate the process by providing the activation energy for reaction (e.g., by making the fixed H/O ratio more reducing by increasing the temperature).

Although the process proposed above and in **Figure 8** is based upon the circumstantial evidence from preliminary work on Genesis samples, it opens paths for future investigations, including experiments, that will refine (or invalidate) this hypothesis.

4.4 Synergy of Genesis Samples with Space Weathering Laboratory Experiments

As discussed above, there are many ways in which further TEM investigations and chemical analyses of Genesis solar wind collectors may be of use to modeling *in situ* space weathering. Each Array held conductors, semiconductors and insulators (i.e., three types of intrinsic silicon, diamond-like carbon, sapphire (corundum), and metal films, see Jurewicz et al. 2003). All samples on an array were exposed to solar wind simultaneously. Equivalent sets of collectors were used on individual Arrays to separately sample solar wind having different velocity spectra: i.e., bulk, fast, slow, or CME solar wind. During solar wind exposure, each collector equilibrated at a temperature dependent upon its optical properties, but the total variation of temperature among (non-metal) collectors during solar exposure was only about 100°C (Jurewicz et al. 2003), which is a small percentage of their melting points. Thus, Genesis samples can, potentially, be used to separately investigate the role of individual factors (e.g., strength of bonds, photovoltaic surface charging, diffusion rates) that control the progression of space weathering.

Genesis sample research has already led to insights into the weathering of the lunar regolith. The depth profile of solar wind Ne in lunar regolith was shown to be a simple solar wind implant modified by surface sputtering during millennia of solar wind implantation (Grimberg et al. 2006). This early work used SRIM to model the expected SW implants. SRIM models have been useful to the study of Genesis space weathering, both by (i) predicting ideal depth profiles and (ii) for highlighting observed deviations from those predictions. Specifically, SRIM has successfully predicted depth profiles of minor solar wind ions in the Genesis amorphous diamond-like carbon (e.g., Jurewicz et al. 2020 supplementary material) and bulk metallic glass (Grimberg et al. 2006). In contrast, SRIM depth-profile predictions have not accurately matched implant profiles from the Genesis silicon, except – perhaps – for SW H (Figures 2a and 1, this text).

Optical properties of post-flight Genesis collectors can be compared with pre-flight counterparts using ellipsometry. Developing ellipsometry models using TEM to characterize the local radiation damage in Genesis collectors will not only help Genesis researchers to choose samples for specific projects but may provide insight into understanding some spectra from airless bodies. Importantly, it is also plausible that understanding the changes in the optical properties incurred by Genesis materials during flight will aid the design of laboratory experiments targeting space weathering, as well as the interpretation of their results.

One issue with laboratory work on space weathering is that the natural solar wind implant currents are too low to effectively reproduce. The implantation of SW H into Genesis materials at the L1 point ranged from ~0.033 – 0.040 nA/cm^2 for fluences ranging from 4×10^{15} to 1.6×10^{16} ions/cm^2 (Jurewicz et al. 2021b) at exposure times ranging from many months to over two years. Irradiations for space weathering research use much higher implant currents for practical reasons (e.g., Laczniak et al. 2022). (1) Ion beams with lower currents tend to be unstable in terrestrial laboratories. (2) The duration of exposure to replicate a 1.6×10^{16} ions/cm^2 implant is too long. (3) Implanting ions at the solar wind spectrum of energies and doses of multiple solar wind ions (if possible) would be sequential, not concurrent. Thus, any diffusion rates measured could, in theory, be dependent upon the order of implantation. In some ways, putting a suite of geologically interesting materials into an array (as per Genesis) and flying them on the Deep Space Gateway (Wiens et

al. 2018) or another spacecraft outside of Earth's magnetic field might be a more accurate way to extend what we can learn about space weathering.

But what if that long duration required for forming space weathering features *in situ* is primarily the wait for the amorphous layer to nucleate and begin to grow? Then, perhaps, we can decrease the duration of laboratory-based experiments by starting with materials already having a (fabricated) thin amorphous film.

The semi-conductor industry routinely creates amorphous silicon layers to precise thicknesses. Using those techniques and, perhaps, others such as polishing, or depositing thin films (Mavrič et al. 2019), it may be possible to create amorphous or partially amorphous layers on other materials. Then, laboratory experiments using simulated solar wind energies can be designed to check if amorphous or partially-amorphous layers thicken to the depth of the peak of subsequent radiation damage, and then slowly thicken as the solar wind ions and damage accumulate (e.g., Steps 2 – 3 of **Figure 8**). Once ellipsometry is made useful for finding amorphous layers, perhaps experiments that try to "thicken" the amorphous layers can be done by implanting low-energy H into flown Genesis samples.

If thick amorphous layers are formed in the laboratory, other ideas presented earlier in this Discussion section can also be tested. For example, the depth profiles of low energy implants into amorphous materials can be measured and compared to SRIM, and changes in their shape and composition with heating or electrical potential can be measured. Or, if a hydrogen-rich glass of an Fe-bearing silicate mineral is irradiated with low-energy H, perhaps it can be shown whether nanophase Fe eventually precipitates under the experimental conditions (e.g., Steps 4 – 5 of **Figure 8**).

None of the Genesis collector materials contain significant Fe, so the development of nanophase Fe precipitates cannot be studied directly using Genesis samples. There is one collector containing Ni. That collector is a bulk metallic glass (BMG) with a bulk composition of $Zr_{58.5}Nb_{2.8}Cu_{15.6}Ni_{12.8}Al_{10.3}$ atom % (Grimberg et al. 2008 supporting online material). The BMG was positioned so that it covered the Genesis Array deployment mechanism, so it was only used to capture bulk solar wind. On the other hand, (1) it is possible that the Ni will behave as an Fe analog, (2) the BMG was

inhomogeneous structurally, containing both glass and dendrites. Thus far, no one has characterized either the Genesis flight spare or flown BMG using TEM.

5. SYNOPSIS

Exposure to solar wind at the L1 point has changed optical, chemical, and structural properties of the Genesis mission collector materials. This "space weathering" occurred in only a few years under relatively hot conditions and a low solar wind flux. The effect of the solar wind irradiation depended upon the collector material and the conditions of exposure.

Radiation-enhanced segregation was observed in Genesis silicon. Many collectors showed amorphous layers, which may have existed pre-flight from polishing. Amorphous layers in silicon and nanocrystalline layers in sapphire seen in TEM were all the thickness of the SW H peak, regardless of the solar wind energy spectrum to which the collector was exposed. Elements that – pre-flight- were predicted to diffuse rapidly and exchange with the surface were retained at solar fluences – the only recognized exception being SW Na in silicon.

Genesis "space weathering" was discovered because the crash of the Genesis spacecraft upon landing meant that Genesis PIs had to learn how to clean the surfaces of collector fragments in a manner that ensured the near-surface solar wind implant was not disturbed. This cleaning effort revealed chemical anomalies from flight. Similarly, both TEM studies of structure and ellipsometry measurements of optical properties were sponsored by Genesis Curation to develop methods for non-destructive sample characterization. So, thus far, the space weathering research has been incidental to other Genesis-related goals. But this reconnaissance work suggests that Genesis samples may be a significant resource for studies of space weathering by future researchers. Using Genesis samples would allow comparison of different materials exposed to the same solar wind irradiation conditions, as well as the same material exposed to different solar wind velocity distributions. Thus, a systematic study comparing Genesis flown collectors, Genesis flown but not exposed samples, and flight spare collectors could indicate changes due to solar wind exposure as a function of composition, structure, and other material properties. Laboratory experiments could then assess the viability

of processes suggested by sample studies. Indeed, future work might inspire a new flight project to further define the processes of space weathering at low ion currents and simultaneous implantation of solar wind ions at a variety of energies.

6. ACKNOWLEDGEMENTS

Many thanks to the two anonymous reviewers of this manuscript. Following their comments and suggestions added clarity and simplified the structure.

7. REFERENCES[9]

Abe, H., Yamamoto, S., & Naramoto H. 1997 NIMPB **127/128** 170

Allton, J. H., Calaway, M. J., Nyquist, L. E., Jurewicz, A. J. G., & Burnett, D. S. 2018 LPSC ***49*** *1671*

Allton, J. H., Keller, L. P., Rahman, Z., et al. 2019 LPSC **50** *1118*

Allton, J. H., Gonzalez, C. P., Allums, K. K., et al. 2022 LPSC **53** 1574

Allums, K. K., Jurewicz, A. J. G., Olinger, C. T., et al. 2020 LPSC ***51*** *2768*

Bochsler, P. 2007, A&ARv 14:1–40 DOI: 10.1007/s00159-006-0002-x

Burnett, D. S., Woolum, D. S., Jurewicz, A. J. G., et al. 2007 LPSC **38** 1943

Burnett, D. S., Jurewicz, A. J. G. & Woolum, D. S. 2019 M&PS. **54**(5) 1092 DOI:10.1111/maps.13266

Calaway, M. J., Stansbery, E.K., McNamara, K.M. 2006 LPSC **37** 1420

Calaway, M. J., Stansbery, E. K., & Keller, L. P. 2009, NIMPB **267** 1101 DOI: 10.1016/j.nimb.2009.01.132

Dienes, G. J. & Damask, A. C. 1958 JAP 29 1713 doi: 10.1063/1.1723032

Flynn, C., Atanackovic, P., & Enjeti L. 2012, NIMPB **285** 112 DOI: 10.1016/j.nimb.2012.05.004

Grier, J., & Rivkin, A. S. 2018, in Airless bodies of the inner solar system: *Understanding the Process Affecting Rocky, Airless Surfaces* (Elsevier), **Chapter 6** 121. DOI: 10.1016/C2015-0-04693-7

Grimberg, A., Baur, H., Bochsler, et al. 2006 Sci **314** 1133 DOI: 10.1126/science.1133568

Grimberg, A., Baur, H., Bühler, F., Bochsler, P., & Wieler, R. 2008 GeCoA **72** 626 DOI: 10.1016/j.gca.2007.10.017

Heber, V. S., Olinger, C., Baur, H., Burnett, D. S. & Wieler, R. 2008 LPSC **39** 2327

Heber, V. S., Wieler, R., Baur, H., et al. 2009 GeCoA 73, 7414

[9]URL for online LPSC abstracts is written as: https://www.usra.edu/meetings/lpscABCD/pdf/WXYZ.pdf, where ABCD is the year of the conference and WXYZ is the abstract number.

Heber, V. S., McKeegan, K. D., Burnett, D. S., et al. 2014, ChGeo, 2014, **390** 61 DOI: 10.1016/j.chemgeo.2014.10.003

Heber, V. S., McKeegan, K. D., Steele, R. C. J, et al. 2021, ApJ **907** 15 DOI: 10.3847/1538-4357/abc94a

Humayun, M.,Burnett, D. S. & Jurewicz, A. J. G. 2011 LPSC **42** *1211*

Hirschmann, M. M. 2021 GeCoA **313** 74

Huss, G. R., Nagashima, K., Burnett, D. S., et al. 2012 LPSC **43** 1709

Huss, G. R., Koeman-Shields, E., Jurewicz, A. J. G., et al. 2020 M&PS **55**(2) 326 DOI: 10.1111/maps.13420

Janakiraman Paramasivan, G., Sharma, M. Jurewicz, A. & Burnett, D. 2018 LPSC **49** 2886

Jones S. W. 2000 Diffusion in silicon (published online in 2008 by I. C. Knowledge, LLC)

Jurewicz, A. J. G., Burnett, D. S., Wiens, R. C., et al. 2003, SSRv **102**, 27 DOI:10.1023/A:1024469927444

Jurewicz, A. J. G., Burnett, D. S., Woolum, D. S., et al. 2008 LPSC **39** 2272

Jurewicz, A. J. G., Rieck, K. D., Hervig, R., et al. 2020 M&PS **55**(2) 352 doi: 10.1111/maps.13439

Jurewicz, A. J. G., Olinger, C. T., Burnett, D. S., et al. 2021, JAAS, **36** 194 DOI:10.1039/D0JA00375A

Jurewicz, A. J. G., Laming, J.M., & Christofferson, R. 2021b LPSC ***52*** *1295*

Jurewicz, A. J. G., Burnett, D. S., A. M. Amarsi, & Grevesse N. 2023 LPSC ***54*** 1702.

Keller, L. P., Christoffersen, R., Jurewicz, A. J. G., et al. *2022 LPSC **53** 1196*

King, B. V., Pellin, M. J., & Burnett, D. S. 2008, ApSS **255** 1455 DOI: 10.1016/j.apsusc.2008.05.158

Koeman-Shields, E. C., Huss, G. R., Westphal, A. J., et al. 2017 LPSC **48** 2485

Laming, M., Heber, V. S., Burnett, D. S., et al. 2017, *ApL* **851** L12 DOI: 10.3847/2041-8213/aa9bf0

Laming, J. M., Vourlidas, A., Korendyke, C., et al. 2019 ApJ **879**(2) (16 pp) DOI: 10.3847/1538-4357/ab23f1

Laczniak, D. L., Thompson, M. S., Christoffersen, R., et al. 2022 LPSC **53** 1749

Marty, B., Chaussidon, M., Wiens, R. C., Jurewicz, A. J. G. & Burnett, D. S. 2011 Sci **332** 1533 DOI:10.1126/science.1204656

Mavrič, A., Valanta,M., Cui, C., & Wanga, Z. M. 2019 JNCS *521 119493* Doi: 10.1016/j.jnoncrysol.2019.119493

McKeegan, K. D., Kallio, A. P. A., Heber, V. S., et al., 2011, Sci **332**(6037) 1528 DOI: 10.1126/science.1204636

Meshik, A., Mabry, J., Hohenberg, C., et al. 2007, Sci **318** 433 DOI:10.1126/science.1145528

McNamara, K. M. 2005 *LPSC* **36** 2403

McNamara, K. M. & Stansbery, E. K. 2005 *LPSC* ***36*** *2402*

Nishiizumi, K., Reedy, R. C., Burnett, D. S., Komura, K. & Welten, K. C. 2006 *LPSC* **37** 2420

Olinger, C. T., Dragland, E. J., & Martino, A. J. 2018 *LPSC* ***49*** *2861*

Portsel, L. M., Shuman, V. B., Lavrent'ev, A. A., et al. 2020, Semic, 2020 **54**(4) 393 DOI: 10.1134/S1063782620040120

Reisenfeld, D. B., Gary, S. P., Gosling, J. T., et al. 2001, JGR **106**(4) 5693 DOI:10.1029/2000JA000317

Reisenfeld, D. B., Burnett, D. S., Becker, R.H., et al. 2007 SSRv **130** 79 DOI:10.1007/s11214-007-9215-1

Reisenfeld, D. B., Wiens, R. C., Barraclough, B. L., et al. 2013 SSRv 2013 **175** 125 DOI:10.1007/s11214-013-9960-2

Rieck, K. D. 2015 School of Earth and Space Exploration, Arizona State University [dissertation 2015] https://keep.lib.asu.edu/items/154194

Rieck, K. D., Jurewicz, A. J. G. & Ogliore, R. C. 2021 LPSC **52** 2638

Sharma, M., Janakiraman Paramasivan, G., Jurewicz, A., Burnett, D. 2022 LPSC **53** 2866

Stansbery, E. K. & Genesis Recovery Processing Team. 2005 LPSC ***36*** *2179*

Thompson, M. S., Christoffersen, R., Zega, T. J. & Keller, L. P. 2014 EP&S **66** 1 DOI: 10.1186/1880-5981-66-89

Titov, A. I., Azarov, A. Yu. & Belyakov, V. S. 2003, *Semic* **37**(3) 340 DOI:10.1134/1.1561530

Wiens, R. C., Burnett, D. S., Jurewicz A., et al. 2018 Deep Space Gateway Concept Science Workshop LPI (LPI Contrib. No. 2063)**3151** https://www.hou.usra.edu/meetings/deepspace2018/pdf/3151.pdf